RESEARCH ARTICLE

GCB-BIOENERGY
BIOPRODUCTS FOR A SUSTAINABLE BIOECONOMY

WILEY

Moisture content estimation and senescence phenotyping of novel *Miscanthus* hybrids combining UAV-based remote sensing and machine learning

Giorgio Impollonia[1,2] | **Michele Croci**[1,2] | **Enrico Martani**[1] | **Andrea Ferrarini**[1] | **Jason Kam**[3] | **Luisa M. Trindade**[4] | **John Clifton-Brown**[5,6] | **Stefano Amaducci**[1,2]

[1]Department of Sustainable Crop Production, Università Cattolica del Sacro Cuore, Piacenza, Italy

[2]Remote Sensing and Spatial Analysis Research Center (CRAST), Università Cattolica del Sacro Cuore, Piacenza, Italy

[3]Terravesta, Saxilby, Lincoln, UK

[4]Wageningen University & Research, Plant Breeding, Wageningen, The Netherlands

[5]Institute of Biological, Environmental and Rural Sciences, Aberystwyth University, Aberystwyth, UK

[6]Justus-Liebig-Universität Gießen, iFZ, Gießen, Germany

Correspondence
Giorgio Impollonia, Department of Sustainable Crop Production, Università Cattolica del Sacro Cuore, Piacenza 29122, Italy.
Email: giorgio.impollonia@unicatt.it

Abstract

Miscanthus is a leading perennial biomass crop that can produce high yields on marginal lands. Moisture content is a highly relevant biomass quality trait with multiple impacts on efficiencies of harvest, transport, and storage. The dynamics of moisture content during senescence and overwinter ripening are determined by genotype × environment interactions. In this paper, unmanned aerial vehicle (UAV)-based remote sensing was used for high-throughput plant phenotyping (HTPP) of the moisture content dynamics during autumn and winter senescence of 14 contrasting hybrid types (progeny of *M. sinensis x M. sinensis* [*M. sin x M. sin*, eight types] and *M. sinensis x M. sacchariflorus* [*M. sin x M. sac*, six types]). The time series of moisture content was estimated using machine learning (ML) models and a range of vegetation indices (VIs) derived from UAV-based remote sensing. The most important VIs for moisture content estimation were selected by the recursive feature elimination (RFE) algorithm and were BNDVI, GDVI, and PSRI. The ML model transferability was high only when the moisture content was above 30%. The best ML model accuracy was achieved by combining VIs and categorical variables (5.6% of RMSE). This model was used for phenotyping senescence dynamics and identifying the stay-green (SG) trait of *Miscanthus* hybrids using the generalized additive model (GAM). Combining ML and GAM modeling, applied to time series of moisture content values estimated from VIs derived from multiple UAV flights, proved to be a powerful tool for HTPP.

KEYWORDS
GAM, high-throughput plant phenotyping, machine learning, *Miscanthus*, moisture content, multispectral, remote sensing, senescence, transferability, UAV

1 | INTRODUCTION

Miscanthus is a promising perennial crop that can achieve high biomass production on marginal lands (Amaducci et al., 2016; van der Cruijsen et al., 2021; Pancaldi & Trindade, 2020; Shepherd et al., 2020). Due to its perennial nature, *Miscanthus* has a limited input requirement and is cultivated under no tillage regime leading to multiple ecosystem services provision (Agostini et al., 2021; Ferrarini et al., 2016, 2021; Martani et al., 2021). Most of the research on *Miscanthus* has been conducted on *Miscanthus* x *giganteus* (Heaton et al., 2010), which is a naturally occurring sterile triploid hybrid of *Miscanthus sacchariflorus* (*M. sac*) and *Miscanthus sinensis* (*M. sin*) (Hodkinson et al., 2002). New *Miscanthus* hybrids (Clifton-Brown et al., 2018, 2019; Hastings et al., 2017) have been recently obtained from several breeding programs (Clifton-Brown et al., 2019). In Europe, rhizome- and seed-based *Miscanthus* hybrids are available at a technology readiness level that can enable the plantation of thousands of hectares per year (Clifton-Brown et al., 2018). These novel *Miscanthus* hybrids are being tested in multiple environments within the EU-BBI project GRACE.

Plant senescence is a key trait for perennial plants as it limits biomass yield, modifies moisture content, and affects nutrient translocation (Boersma et al., 2015; Jensen et al., 2016; Malinowska et al., 2016; Sarath et al., 2014; Yang & Udvardi, 2017). Moisture content at harvest is the most important biomass quality trait (Robson et al., 2011; Styks et al., 2020). Monitoring the dynamics of crop senescence and moisture content can support the choice of the optimal harvest time that can improve biomass quality and logistics biomass supply chain. Lewandowski et al. (2016) found that moisture content of different genotypes can vary due to morphological differences and senescence patterns, but it is primarily determined by harvest date. Several studies have shown that late senescence (stay green—SG) maximizes biomass yield (Clifton-Brown et al., 2001), while early senescence increases biomass quality (Clifton-Brown & Lewandowski, 2002). SG is determined by a complex physiological control (e.g., chlorophyll efficiency, nitrogen contents, nutrient remobilization, and source–sink balance) (Munaiz et al., 2020; Thomas & Howarth, 2000) and traditional phenotyping methods for evaluating SG and delayed senescence are time-consuming (Furbank & Tester, 2011). Nondestructive methods are based on greenness visual score (Bogard et al., 2011) and SPAD measurements (Lopes & Reynolds, 2012; Xie et al., 2016), for the estimation of the green leaf area and relative chlorophyll content, respectively. These methods can be used to monitor field trials but are not effective in monitoring senescence dynamics at commercial scale. New sensing technologies

have contributed to a substantial improvement in the monitoring of SG in different crops (Cerrudo et al., 2017; Kipp et al., 2014; Liedtke et al., 2020; Lopes & Reynolds, 2012). High-throughput plant phenotyping (HTPP) with remote sensing is a rapid and nondestructive technology that can be used to monitor the senescence of numerous genotypes, thus supporting breeding programs (Anderegg et al., 2020; Hassan et al., 2018). Remote sensing technologies use different types of sensors, such as Red–Green–Blue (RGB), multispectral, hyperspectral, and thermal cameras, installed on satellites and on unmanned aerial vehicles (UAVs) (Xie & Yang, 2020). Spectral data can be used to calculate vegetation indices (VIs), which can be used to estimate crop parameters related to SG trait: normalized difference vegetation index (NDVI) for green biomass (Cabrera-Bosquet et al., 2011), enhanced vegetation index (EVI) for leaf area index (LAI) (Alexandridis et al., 2019), and modified chlorophyll absorption in reflectance index (MCARI) for chlorophyll content (Haboudane et al., 2002). Other VIs, such as the plant senescence reflectance index (PSRI) (Merzlyak et al., 1999) or the structure insensitive pigment index (SIPI) (Peñuelas et al., 1995), which are based on the chlorophyll/carotenoid ratio as the decomposition rates of these pigments are affected during senescence, were specifically developed to study crop senescence. The normalized difference water index (NDWI) (Gao, 1996), calculated using near-infrared (NIR) and shortwave-infrared (SWIR) spectral bands, has been proposed as a powerful direct water-sensitive VI, which can be used for the remote sensing of canopy water content (CWC) (Jackson et al., 2004). However, NDWI is rarely calculated by UAV because it requires costly sensors that are equipped with the SWIR band. Zhang and Zhou (2019) compared direct against indirect (which does not include the SWIR band) water-sensitive VIs, such as NDVI, NDRE, CIgreen, and CIred-edge and found that these VIs were strongly correlated with the CWC as the direct VIs.

Field trials carried out with small plots cannot be monitored using satellite data, for this HTPP using UAV-based multispectral images is best used in breeding programs where numerous genotypes are compared (Gracia-Romero et al., 2019; Ostos-Garrido et al., 2019; Su et al., 2019; Varela et al., 2021; Yang et al., 2017; Zhou et al., 2019). UAV-based multispectral images were used in many studies to compare genotypes on the basis of VIs linked to LAI (Potgieter et al., 2017), green LAI (Blancon et al., 2019), canopy cover (Makanza et al., 2018), crop biomass and yield (Johansen et al., 2020; Wang et al., 2019), and senescence dynamics (Hassan et al., 2018). However, many VIs show nonlinear relationships with their associated crop parameters (Verrelst et al., 2015). Machine learning (ML) regression algorithms have increasingly been used in HTPP to recognize nonlinear and nonparametric relationships. ML is

used to combine multiple VIs for estimating crop parameters from a sequence of UAV remote sensing acquisitions. ML models use two main datasets: a training set on which the best model is trained to fit the measured parameters and a test set used to assess the performance of model (Kuhn & Johnson, 2013). In addition to the VIs data, with ML methods, numerous types of data, such as categorical variables (e.g., genotype, crop type, locations, agronomic treatments) (Im et al., 2009; Meroni et al., 2021; Wolanin et al., 2020), can be used in the analysis (Verrelst et al., 2018). An ML method commonly used in many remote sensing analyses is random forest (RF) (Belgiu & Drăguţ, 2016; Holloway & Mengersen, 2018), which can estimate crop biomass (Han et al., 2019) and yield (Johansen et al., 2020) from UAV multispectral images. A main limit of the RF model is its transferability to environments, cropping systems, or growing seasons different from those used for training the model (Vuolo et al., 2013). Another limitation is in the training set size (Millard & Richardson, 2015) and the unreliability of predictions made beyond the range of values of the parameters present in the training set (Shah et al., 2019). In addition, Schauberger et al. (2020) reported that 52% of the studies on ML do not validate the models' performance with independent test sets. Overall, the quality of training data for developing robust ML models is the key for successfully transferring the trained model and its knowledge to other target domains/tasks. For these reasons, new studies are needed to assess the transferability of ML models for UAV applications in agricultural sciences (Johansen et al., 2020).

However, to date, only time series VIs data from UAV, and not estimated crop parameter of ML models, are used for HTPP. A set of known models are normally fitted to VIs time series to characterize plant growth/status associated with different phenological phases. Specifically for the senescence, logistic functions (Christopher et al., 2014) and the Gompertz model (Anderegg et al., 2020) are the two most used models. Another potential approach to fit VIs data is the generalized additive model (GAM) (Nolè et al., 2018). Antonucci et al. (2021), for example, successfully used GAM approach for HTPP of whole-canopy photosynthesis and transpiration.

Although remote sensing applications that support these approaches exist and have been already tested successfully for field crops (Alam et al., 2012; Kavats et al., 2019; Yang, 2011; Zhang et al., 2021), no remote sensing application for estimating moisture content of *Miscanthus* is reported in scientific literature.

As a first-time testbed for phenotyping *Miscanthus* with UAV remote sensing, two locations, where 14 contrasting *Miscanthus* hybrids were compared in a completely randomized block design, were monitored regularly with moisture content measurements and UAV flights and senescence dynamics were assessed during two growing seasons. The objectives of this study were (1) to evaluate the performances and transferability of RF models in estimating the moisture content of *Miscanthus* biomass and (2) to phenotype the dynamics of senescence and identify SG trait of contrasting *Miscanthus* hybrids using GAM applied to moisture content time series.

2 | MATERIALS AND METHODS

2.1 | Experimental design

This study is part of the EU-BBI funded project "GRowing Advanced industrial Crops on marginal lands for biorEfineries" (GRACE) that aims to prove the feasibility of large-scale *Miscanthus* cultivation on marginal land. Two of the eight plot scale (PS) trials conducted within GRACE project have been selected for this study. The two sites were located in the province of Piacenza (NW Italy): PAC 1 located in San Bonico (45°00′11.70″N, 9°42′35.39″E) and PAC 2 located in Chiulano (44°50′40.32″N, 9°35′04.93″E) (Figure 1). Former land use was arable land with cereal crops rotation and permanent meadow, respectively, in PAC 1 and PAC 2. The climate in both locations is temperate. The sites differ for soil type and elevation (Figure 1). Meteorological data were collected from automatic weather stations located at each experimental site (Table 1). Experimental layout was a complete randomized block design with 14 *Miscanthus* hybrids (Table 2) with $n = 4$ replicates for a total of $n = 56$ plots. Plot size was 6 m × 7 m. The 14 hybrids, coded from GRC 1 to GRC 15 (except GRC 12), were grouped into three main genotypes: *M. x giganteus* as control genotype, and interspecific (*M. sin x M. sac*) and intraspecific (*M. sin x M. sin*) hybrids genotypes. Both PS trials were established in April 2018 after winter ploughing and spring seed bed preparation (power harrowing). Plugs and rhizomes were manually transplanted while mechanical weeding during the first years was performed three times. Neither irrigation nor fertilization was applied. Measurements of this study were carried in the second and third growing season during senescence.

2.2 | Crop measurements

Senescence was tracked visually following the scoring method proposed by Robson et al. (2011), which is based on a scale from 1 to 9, where 1 indicates the lowest level of "greenness" of the whole visible aerial parts of the plant and 9 is the score attributed when no visible leaf senescence occurs. Scores were acquired from August to
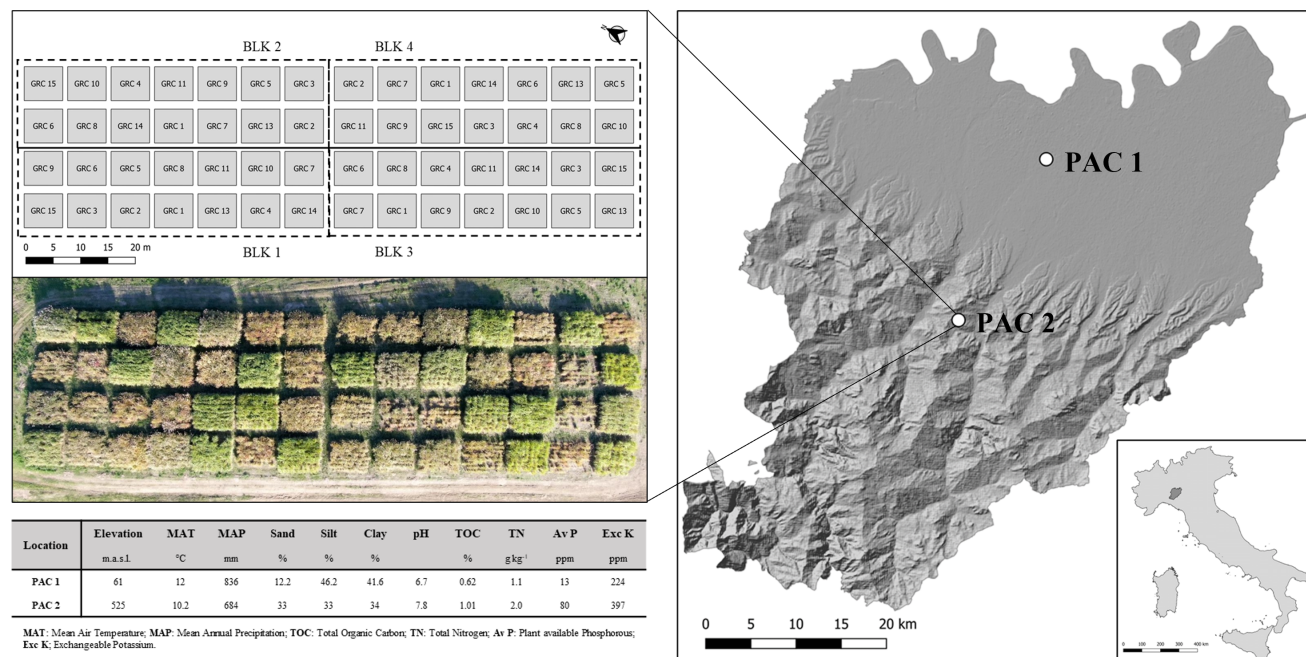
FIGURE 1 Locations, experimental field design, main soil properties and drone picture of *Miscanthus* trials

February (until harvest) for a total of 10 events in PAC 1 and 9 in PAC 2. Besides scoring senescence, at each measurement event, whole stem samples randomly selected for each plot (20 for *M. sin x M. sin* and 10 for *M. sin x M. sac* hybrids, respectively) were sampled to calculate plant moisture content. Samples were weighed immediately after harvest and again after having been oven-dried at 105°C, and then, the percentage of moisture content was calculated (Samuelsson et al., 2006).

2.3 | UAV multispectral data and vegetation indices

The unmanned aerial vehicle (UAV) used in the experiment was a four-rotator DJI Matrice 210 RTK (SZ DJI Technology Co.) combined with an RTK (Real-Time Kinematic) GPS positioning system. At each visual scoring event, a UAV multispectral data acquisition was performed; in addition, 10 supplementary flight missions were carried out on PAC 1 and five on PAC 2 to increase the frequency of senescence tracking. Ten flights were performed over PAC 1 in both seasons, while in PAC 2, 6 and 8 flights were realized in the first and second seasons, respectively (Table S1). The UAV was equipped with a MicaSense RedEdge-Mx multispectral camera (MicaSense). RedEdge-Mx camera can acquire the images in five different spectral bands: blue (475 nm center, 32 nm bandwidth), green (560 nm center, 27 nm bandwidth), red (668 nm center, 14 nm bandwidth), red edge (717 nm center, 12 nm bandwidth) and near-infrared (840 nm center, 57 nm bandwidth). All the flights were performed between 11.00 and 15.00. The flight altitude above ground level (AGL) was 40–50 m in PAC 1 and 80–100 m in PAC 2. The forward overlap was set at 80% and lateral overlap was set at 75% of the images. The flight speed was set at 3 m/s. The ground sampling distance (GSD) was 2.78–3.47 cm and 5.56–6.94 cm in PAC 1 and PAC 2, respectively. The flight was performed in automatic mode with way-point routes as the presence of a GPS navigation system enables a more accurate image acquisition. The DJI Pilot software (SZ DJI Technology Co.) was used for flight planning and automatic mission control. For the radiometric calibration of the images, the reflectance of a spectral panel (MicaSense) with reflectance values provided by MicaSense was captured before each flight. In addition, a light sensor that automatically adjusts the readings to ambient light was mounted at the top of the UAV to minimize error during image capture. The radiometric calibration, image mosaicking, and ortho-mosaic generation were done using the Pix4D mapper (Pix4D, S.A.). The orthomosaic in reflectance values generated from the software was used for the calculation of 54 vegetation indices (VIs) as shown in Table S2. To extract the spectral information of each experimental plot, the polygons of the experimental design were drafted in AutoCAD (Autodesk) and georeferenced based on the UAV multispectral images by using QGIS software (QGIS Development Team, 2021).

TABLE 1 Mean monthly temperature, humidity, and rainfall in the two locations considered during the two seasons

Location	Season	Month	Temperature			Humidity			Rainfall (mm)
			Mean (°C)	Max (°C)	Min (°C)	Mean (%)	Max (%)	Min (%)	
PAC 1	2019	September	19.8	20.2	19.3	76.4	78.5	74.2	79.2
		October	15.5	15.8	15.2	90.1	91.3	88.8	120.6
		November	8.7	8.9	8.5	97.4	97.9	96.9	231.0
		December	4.9	5.2	4.6	91.6	92.6	90.6	73.4
		January	2.9	3.2	2.5	94.1	95.1	93.1	17.8
		February	6.7	7.2	6.2	75.3	77.2	73.3	1.2
	2020	September	20.5	21.0	19.9	73.6	76.1	71.1	18.6
		October	13.1	13.5	12.8	87.4	89.0	85.7	103.8
		November	8.2	8.5	7.9	95.4	96.2	94.6	24.4
		December	3.3	3.5	3.1	99.1	99.3	98.9	216.8
		January	1.5	1.8	1.2	92.5	93.5	91.5	10.4
		February	4.6	4.9	4.3	96.7	97.3	95.9	0.0
PAC 2	2019	September	18.0	18.4	17.7	75.8	77.6	74.0	65.8
		October	14.2	14.5	14.0	85.2	86.7	83.7	120.0
		November	7.7	8.0	7.5	91.0	92.1	89.7	295.6
		December	5.3	5.5	5.0	80.3	81.6	78.9	83.0
		January	5.1	5.4	4.8	77.6	79.7	75.5	34.0
		February	8.3	8.7	7.9	58.2	60.4	56.3	0.6
	2020	September	16.9	17.2	16.5	72.1	73.9	70.1	19.6
		October	11.7	12.0	11.4	82.9	84.7	81.2	102.6
		November	8.3	8.5	8.1	87.5	88.6	86.3	21.4
		December	2.9	3.2	2.7	95.7	96.4	94.9	146.2
		January	2.0	2.3	1.7	80.3	81.9	78.7	94.8
		February	3.9	4.1	3.7	87.3	88.4	86.2	22.0

TABLE 2 Characteristics of the 14 *Miscanthus* hybrids considered in this study

Material	Hybrid code	Genotype	Planting density
Seed-based plugs	GRC 1–8	*M. sinensis x M. sinensis*	3 plants/m²
Rhizomes[a]	GRC 9	*M. x giganteus*	1.5 plants/m²
Seed-based plugs	GRC 10–14 (except GRC 12)	*M. sinensis x M. sacchariflorus*	1.5 plants/m²
Rhizomes[a]	GRC 15	*M. sinensis x M. sacchariflorus*	1.5 plants/m²

[a]Hybrids commercially available.

2.4 | Machine learning model for moisture content estimation

A recursive feature elimination (RFE) algorithm (Feng et al., 2020; Yue et al., 2018) was initially applied to solve the multicollinearity problem among VIs by selecting the most important VIs for moisture content estimation. Inputs for the RFE algorithm were the predictor variables (the 54 VIs calculated from UAV multispectral images) and the corresponding target values (the measured plant moisture content). In the RFE algorithm, the random forest (RF) model was used to minimize the root mean square error (RMSE). The RFE results were combined with the "*pickSizeTolerance*" function to select a model containing fewer predictor variables within the bounds of a user-defined threshold metric (Parmley et al., 2019). RMSE metric and the 0%, 1%, and 5% tolerance thresholds were utilized to identify models with acceptable performance but with fewer predictor variables.

On the selected VIs, RF was then used to estimate the moisture content of *Miscanthus* hybrids. RF model is an ensemble learning model where the output averages the result of multiple regression trees (Kamir et al., 2020). The RF models were created using the *caret* R package (Kuhn, 2008). Two steps in RF modeling were adopted: Firstly, RF was trained and tested on the VIs selected from RFE algorithm at the tolerance threshold of 1%; secondly, the three categorical crop variables (material, hybrid code, and genotype, Table 2) and their combinations were added in RF modeling to check for improvement in model's performance.

For the RF modeling, the optimal size of the variable subset ("*mtry*") was obtained by grid-searching method using repeated k-fold cross-validation. The repeated *k*-fold cross-validation consists of dividing the data into *k* independent folds of the same size, training the algorithm on (*k*−1) folds, and testing its accuracy on the remaining fold based on the error between predicted and target values several times (Kamir et al., 2020). In our study, we used a tenfold cross-validation, which was repeated five times. This procedure was used to estimate the moisture content and to evaluate the transferability of the models tested on five subset test datasets: four specific season and location

datasets (two locations x two growing seasons) and one reference dataset, as a comparison. The reference dataset was created by using a stratified random sampling method (Han et al., 2019): data from both locations and seasons were split into 70/30 between training and testing based on moisture content distribution. To include the categorical variables into the models (second step), a one-hot-encoded approach was used to encode categorical variables into numbers, assigning the value 1 when the condition is satisfied and 0 when it is not satisfied.

RF models' performances were evaluated calculating the root mean square error (RMSE) and the normalized root mean square error (NRMSE) as follows:

$$\text{RMSE} = \sqrt{\frac{\sum_{i=1}^{n}(x_i - y_i)^2}{n}}$$

$$\text{NRMSE}(\%) = \frac{\sqrt{\frac{\sum_{i=1}^{n}(x_i - y_i)^2}{n}}}{\bar{y}} 100$$

where *n* is the sample number, x_i and y_i are the estimated and measured moisture content, and $\bar{y}$ is the mean of the measured value. The performance metrics were also calculated for different intervals of moisture content and each *Miscanthus* hybrid. The moisture content intervals investigated were lower than 30%, between 30% and 60%, higher than 60%, and finally between 10% and 80%. The set size used for each training dataset was reported to compare the metrics of the models. For each model, the RMSE and NRMSE were calculated for each genotype and for the different moisture content intervals to evaluate the models.

2.5 | GAM for phenotyping *Miscanthus* senescence dynamics

The moisture content during senescence was estimated from spectral data acquired by UAV using the validated RF model: This approach was selected to add supplementary flights to the dataset without field

measurements. The validated RF model included as predictor variables the VIs and the three categorical variables. The time series moisture content dataset estimated from RF was fitted against the modified day of the year (DOY). Early and late senescence in *Miscanthus* occur normally in two different years. To overcome the problem of having nonsequential DOY data along the senescence season, moisture content data of January and February were calculated by adding 365 to the DOY of the corresponding year. To phenotype the dynamics of senescence and identify stay-green (SG) trait of the different *Miscanthus* hybrids, statistical analysis of the estimated moisture content time series was carried out via a generalized additive model (GAM). The regression model GAM is a nonparametric extension of the generalized linear model (GLM), which allows the integration of nonparametric smoothing functions and nonlinear fitting of the variables. GAM models were fitted in R package "*mgcv*" (Wood, 2017). The fitted model used fixed factors and a smooth for DOY, based on location, season, and hybrid. GRC 9 (*M. x giganteus*) was used a reference to detect difference between interspecies and intraspecies *Miscanthus* hybrids.

3 | RESULTS

3.1 | Dynamics of moisture content in *Miscanthus* biomass

The frequency distribution of measured moisture content and its variation during the two senescence seasons at two locations are shown in Figure 2 and Figure S1. Overall, the peak of frequency distribution of moisture content values was recorded for all genotypes within the interval between 30% and 60% (Figure 2). *M. sin x M. sin* showed a left-skewed distribution with relatively high-frequency values for moisture content below 30% (Figure 2). Moisture content loss started at the beginning of December at both locations and for all genotypes (Figure S1). *M. sin x M. sac* hybrids showed a higher moisture content (+18% and +6%) than *M. sin x M. sin* hybrids and *M. x giganteus* in both locations from December until harvest in late winter (Figure 2 and Figure S1). On average, *M. sin x M. sac* hybrids and the *M.* x *giganteus* were harvested at 45% and 37% moisture content, respectively (Figure 2 and Figure S1). *M.* sin x *M. sin* hybrids had an average moisture content at winter harvest of 22%. The dynamics of moisture content during senescence are confirmed by visual recording of senescence score based on plant greenness (Figure S2). For all genotypes, the correlation between senescence

score and moisture content indicated that moisture content loss starts when senescence score values of 4 are recorded.

3.2 | Recursive feature elimination of vegetation indices

The optimal number of vegetation indices (VIs) included in the models to minimize RMSE in the estimation of moisture content was obtained by the recursive feature elimination (RFE) algorithm with repeated cross-validation (Figure 3). RFE analysis showed that using four or less VIs led to a moisture content estimation with RMSE values higher than 8% (Figure 3a). With the 0% tolerance threshold, the minimum RMSE (7.4%) was achieved with 30 VIs. However, the use of 20 or more VIs led to a moisture content estimation with a mean RMSE value of 7.4%. On the contrary, with the thresholds of tolerance of 1% and 5%, the optimal number of VIs was 14 (RMSE = 7.5%) and 6 (RMSE = 7.8%), respectively (Figure 3a). The threshold of tolerance of 1% was chosen as the threshold that maximizes the model's performances with the minimum number of VIs. According to the importance of the ranking (Figure 3b), 14 VIs have been selected for RF models training among the 54 VIs calculated (Figure 3b). The 14 VIs were BNDVI, GDVI, PSRI, MCARI/MTVI2, GOSAVI, NGBDI, NLI, GBNDVI, GLI, MCARI/OSAVI2, SIPI, MCARI2, OSAVI2, and GI. The six most important VIs to reach 5% tolerance (RMSE <7.8%) were (Figure 3b) BNDVI, GDVI, PSRI, MCARI/MTVI2, GOSAVI, and NGBDI.

3.3 | RF model performance and transferability

The performances (RMSE and NRMSE) of the random forest (RF) models were compared among the season-specific datasets of the two location and against one reference dataset (split into 70/30 training/test) (Table 3). When all the genotypes and all moisture content intervals were considered, the RF model of the reference dataset was the most accurate one among the five models considered in estimating *Miscanthus* moisture content (RMSE = 6.9% and NRMSE = 14%). The other models achieved lower accuracy values with RMSE ranging from 9.2% to 10.6% and NRMSE from 20.1% to 22.1%. The accuracy of the RF models trained with the season–location-specific datasets and for the intervals of moisture content of 30%–60% and >60% was on average similar
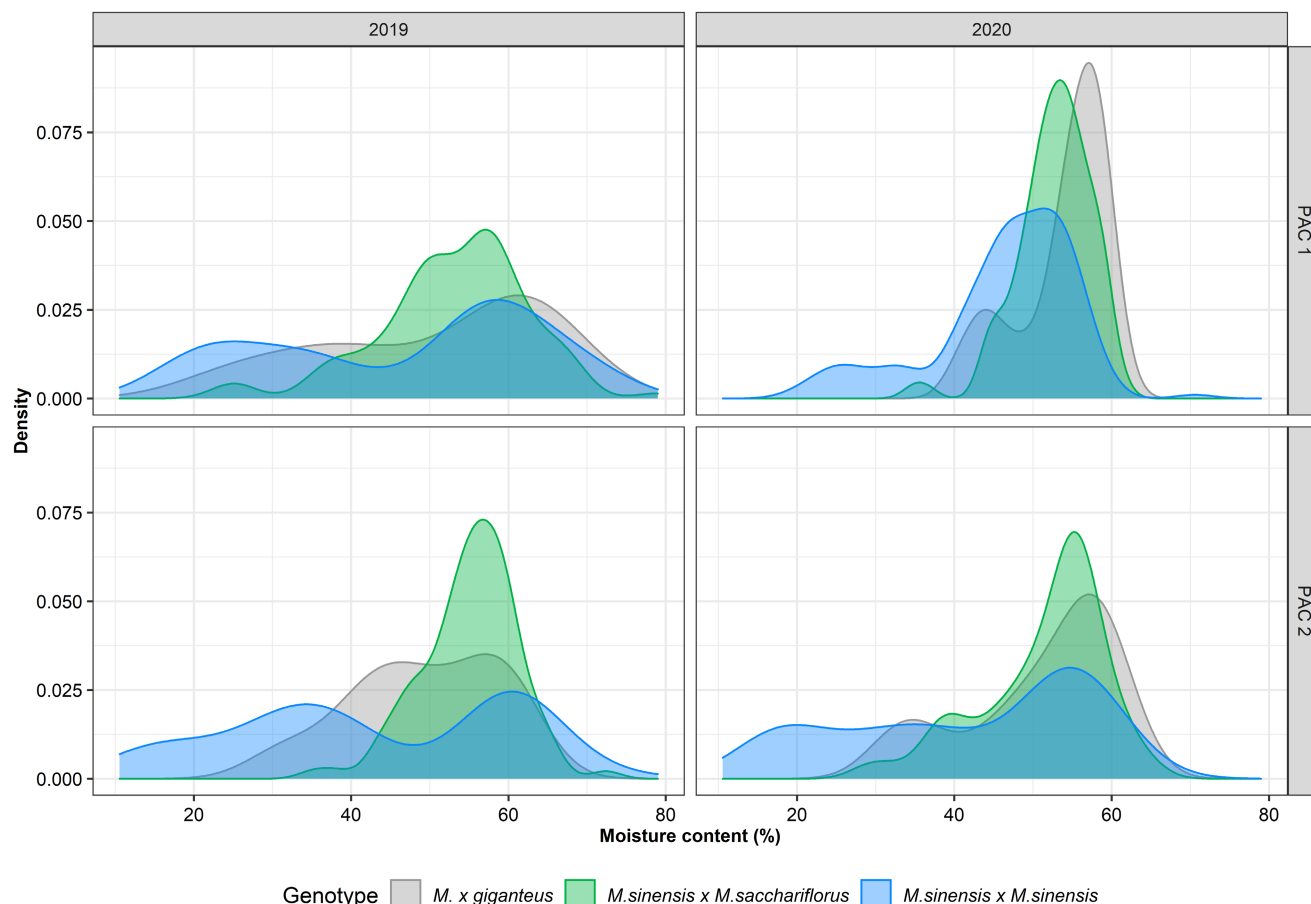
FIGURE 2 Frequency distribution of the moisture content of different *Miscanthus* genotypes during the two seasons and on two locations

(RMSE = 8.5%) to the accuracy of the RF model trained with the reference dataset for the same intervals (RMSE = 6.3%). On the contrary, the accuracy of the RF models for the season–location-specific datasets was lower for the interval of moisture content <30% (RMSE = 16.4%) than the reference dataset (RMSE = 10.7% and 6.3%, respectively).

The addition of categorical variables (material, hybrid code, and genotype of Table 2) to the reference dataset model of VIs improved the accuracy of moisture content estimation (Figure 4). The single addition of material, hybrid code, or genotype in the model (Figure 4b–d) decreased the RMSE from 6.9% (model with only Vis) to 6.8%, 6.4%, and 5.7%, respectively. The simultaneous addition of three categorical variables to the model achieved the best performance with an RMSE = 5.6% and NRMSE = 11.4% (Figure 4e). Finally, the RMSE of all models was evaluated for each genotype (Figure 4f). The addition of categorical variables decreased the RMSE value with respect to the model with only VIs for the *M. x giganteus* genotype from 7.6% to 5.6%, for the interspecific *M. sin x M. sac* genotype hybrids from 6.9% to 4.7%, while for intraspecific *M. sin x M. sin* genotype hybrids from 6.8% to 6.1%.

3.4 | Phenotyping of *Miscanthus* senescence dynamics with multiple UAV flights

The RF model trained with the VIs and the three categorical variables was used to estimate moisture content of *Miscanthus* hybrids from spectral data of multiple UAV flights at two locations. Generalized additive model (GAM) was applied to time series moisture content data estimated from RF model, with the *M. x giganteus* (GRC 9) as reference for estimating significant differences among the hybrids during senescence. *M. sin x M. sin* hybrids (GRC 1–8) from DOY 280 (mid-early October) showed a constant and significant lower moisture content than the *M. x giganteus* hybrid (Figure 5). The first genotype showing a significant difference in moisture content compared to GRC 9 was GRC 5, at DOY 260 (mid-September), while the last was GRC 1, at DOY 312 (mid-early November). Intraspecies *M. sin x M. sin* hybrids showed the highest variability on moisture content loss during senescence compared to interspecies *M. sin x M. sac* hybrids. The estimated difference of moisture content at harvest varied from 10.2% for GRC 1 to 14.5% for GRC 6. On the contrary,
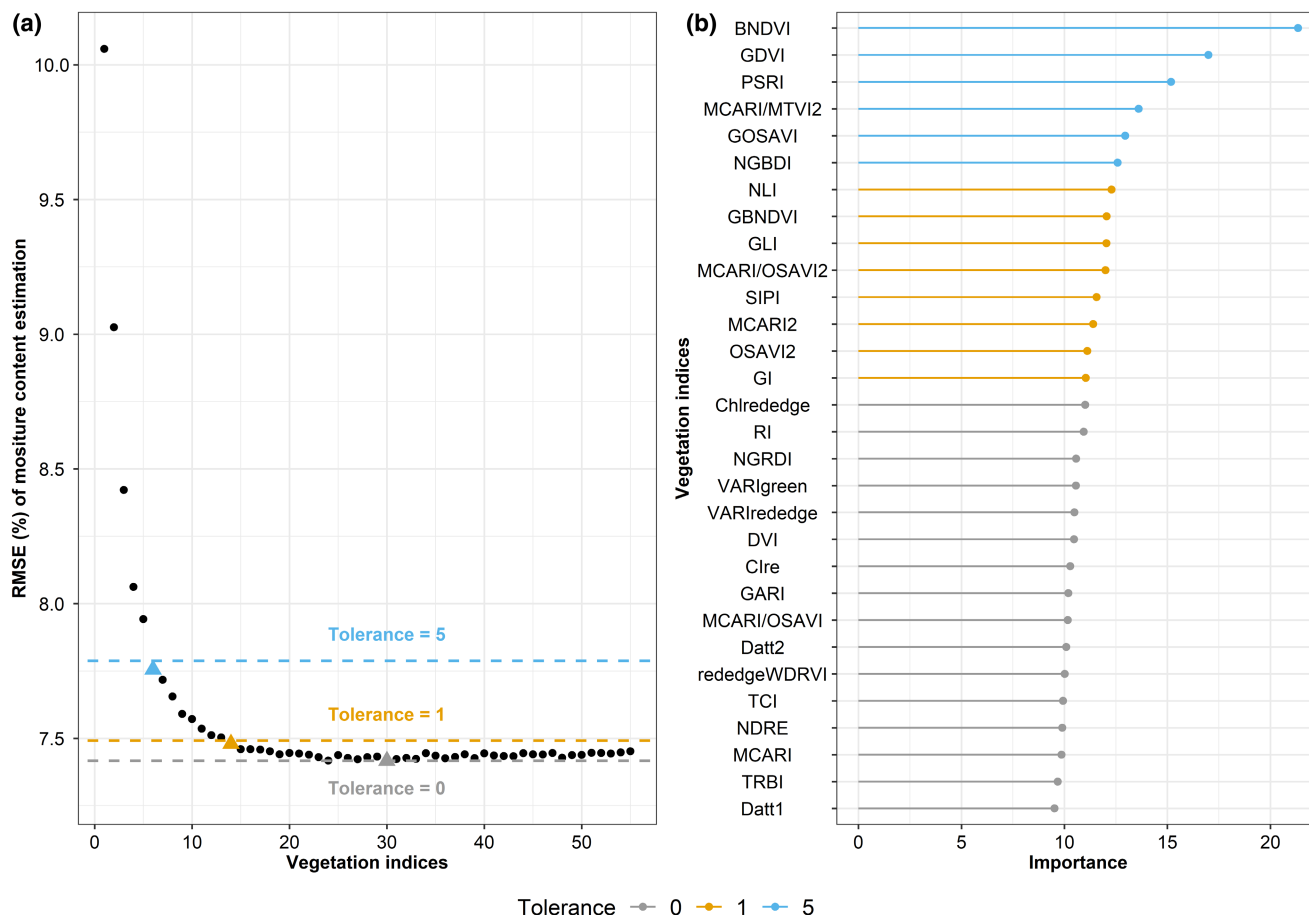
FIGURE 3 (a) Results of the RFE algorithm with different tolerance thresholds and (b) importance of the VIs used in the different tolerance thresholds (blue = 5%, yellow = 1% and grey = 0%)

constant negative differences compared to GRC9 occurred later in the season (early November) for interspecific *M. sin x M. sac* hybrids (GRC 10–15). The difference is statistically significant approximately from DOY 295 (mid-late October) for GRC 10 hybrid and from DOY 314 (mid-early November) for GRC 13 hybrid. At harvest, the estimated moisture content difference varied from −9.2% for GRC 11 to −10% for GRC 14. The rhizome-based GRC 15 hybrid, a *M. sin x M. sac* genotype, showed a similar moisture content dynamics to the other rhizome-based hybrid (GRC 9).

4 | DISCUSSION

The characterization of moisture content dynamics of *Miscanthus* biomass is important to determine the harvest time and selecting the most suitable genotypes in each environment. This study estimated the moisture content of 14 contrasting *Miscanthus* hybrids combining unmanned aerial vehicle (UAV) remote sensing and machine learning. The random forest (RF) model was trained with moisture content values measured directly from each plot

trial, UAV multispectral data (the vegetation indices), and categorical variables of *Miscanthus* hybrids (material, hybrid code, and genotype). The time series of the moisture content values estimated by RF model from VIs derived from multiple UAV flights was used for phenotyping senescence dynamics and identifying the stay-green (SG) trait of *Miscanthus* hybrids using the generalized additive model (GAM).

4.1 | Selection of multispectral vegetation indices for *Miscanthus* moisture content estimation

Increasing the number of VIs from 1 to 14 improved the RF model's accuracy and allowed to decrease RMSE from 10% to 7.5% (Figure 3a). Generally, the estimation of the crop parameters via multiple VIs is affected by data redundancy and multicollinearity among some vegetation indices (VIs) (Yue et al., 2018). The use of recursive feature elimination (RFE) algorithm proved to be a suitable approach to minimize RMSE while reducing the noise effect caused by data redundancy and multicollinearity, as

TABLE 3 Results of the RF models performance according to location, season, moisture content intervals, and genotype (blue = *M. sin* x *M. sin*, grey = *M. x giganteus* and green = *M. sin* x *M. sac*)

Location	Season	Intervals of moisture content (%)	*M. sin x M. sin* n	RMSE	NRMSE	*M. x giganteus* n	RMSE	NRMSE	*M. sin x M. sac* n	RMSE	NRMSE	All genotypes n	RMSE	NRMSE
PAC 1	2019	$x < 30$	81	19.7	87.5	0	18.4	75.9	2	21.0	83.8	83	19.7	86.7
		$30 \leq x \leq 60$	296	6.1	12.5	49	5.9	13.1	249	6.4	12.5	594	6.2	12.5
		$x > 60$	45	11.9	18.1	6	10.0	15.8	26	9.4	14.4	77	11.0	16.9
		$10 \leq x \leq 80$	422	12.2	26.2	55	9.6	19.0	277	7.9	14.9	754	10.6	21.6
	2020	$x < 30$	105	4.5	18.2	2			5			112	4.5	18.2
		$30 \leq x \leq 60$	229	8.8	18.2	40	11.8	22.1	228	11.6	22.0	497	10.2	20.2
		$x > 60$	83	12.2	17.2	13	4.7	7.7	44	6.0	9.7	140	8.3	12.9
		$10 \leq x \leq 80$	417	8.5	18.4	55	11.6	21.5	277	11.5	21.9	749	9.9	20.2
PAC 2	2019	$x < 30$	84	22.7	113.2	2			5			91	22.7	113.2
		$30 \leq x \leq 60$	303	9.0	20.7	43	4.6	9.8	247	5.2	9.8	593	7.0	14.5
		$x > 60$	48	8.4	13.3	11	4.6	7.7	25	6.3	10.0	84	7.6	12.1
		$10 \leq x \leq 80$	435	13.6	31.7	56	4.6	9.4	277	5.4	9.9	768	10.6	22.1
	2020	$x < 30$	84	19.2	93.0	2			3			89	18.8	88.9
		$30 \leq x \leq 60$	288	5.6	11.6	45	9.2	18.5	254	4.8	9.3	587	5.7	11.4
		$x > 60$	76	5.8	9.4	12	3.5	5.8	40	6.7	10.7	128	5.9	9.5
		$10 \leq x \leq 80$	448	11.1	26.6	59	8.7	17.0	297	5.1	9.9	804	9.2	20.1
Reference dataset[a]		$x < 30$	89	10.8	51.8	1	10.8	43.3	3	8.9	32.3	93	10.7	50.0
		$30 \leq x \leq 60$	260	5.1	10.5	41	7.8	15.7	227	7.1	13.5	528	6.3	12.5
		$x > 60$	61	7.3	11.6	10	5.0	8.1	31	4.7	7.4	102	6.3	10.0
		$10 \leq x \leq 80$	410	6.8	14.9	52	7.6	14.9	261	6.9	12.9	723	6.9	14.0

Abbreviations: *n* is the training set size; NRMSE, normalized root mean square error (%); RMSE, root mean square error (%).

[a]Reference dataset is composed of 30% of the initial dataset (both locations and seasons) used for the validation and 70% used for RF model training.
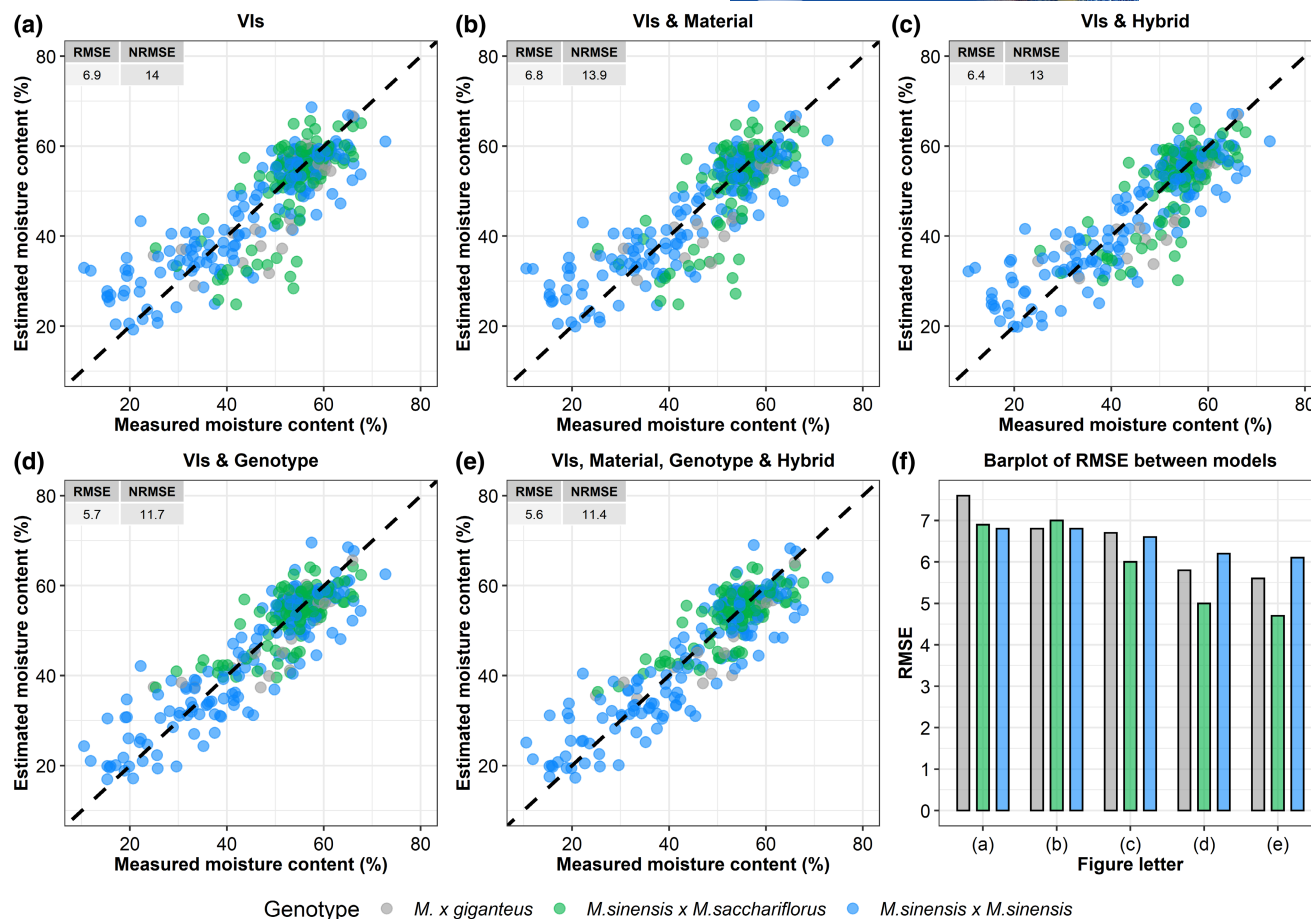
FIGURE 4 Estimated versus measured moisture content (%) of *Miscanthus* with RF model with only VIs and no categorical variables (a), with the addition of transplanting material (b), of hybrid (c), of genotype (d) and their combination (e). RMSE for each model is reported as barplot (f) according to the different genotypes

suggested by Han et al. (2019) and Anderegg et al. (2020). This study showed that the three most important VIs for estimating moisture content were VIs based on blue (BNDVI), green (GDVI), and red-edge (PSRI) spectral bands (Figure 3b). Zhu et al. (2019) found that the blue band is sensitive to the change of carotenoid content and the green and red-edge bands are sensitive to the change of chlorophyll content. VIs based on these spectral bands indeed have been used to study crop senescence dynamics (Anderegg et al., 2020; Peñuelas & Inoue, 1999). The blue band proved to be the most important variable for predicting harvest date (pod's maturity) in soybean (Yu et al., 2016). Anderegg et al. (2020) reported that the time series of PSRI could accurately track senescence dynamics of the canopy of wheat and replace the visual scorings. Furthermore, the SIPI was strongly correlated with relative water content (RWC) and can indirectly evaluate leaf water stress (Peñuelas & Inoue, 1999). Also, this study confirmed that the VIs selected by the RFE algorithm and used in the RF model were sensitive to changes of chlorophyll/carotenoid ratio during senescence. Finally, although no VIs based on the SWIR band were used in

this study, it was demonstrated that the combination of multiple VIs based on VIS-NIR images compensated for the lack of the SWIR band, which is known to predict well crop moisture content when integrated with VIs such as NDWI (Zhang & Zhou, 2019).

4.2 | Moisture content estimation with a machine learning algorithm

This study estimated the moisture content with the RF model, trained with a wide range of genotypes, across two senescence seasons and at two different locations, differing strongly in soils and slightly in climate. These differences, as suggested by Maxwell et al. (2018), help to assess the RF model transferability. The transferability of the moisture content estimation models was evaluated by splitting the moisture content dataset into five test datasets. The performance metrics of the RF models showed that a good accuracy (6.9% of RMSE and 14.0% of NRMSE) was achieved when all the genotypes and all moisture content intervals were considered in the models

(Table 3). Similar results were reported by Li et al. (2021) to estimate the moisture content of three species of trees, who achieved an NRMSE between 8.6% and 13.9%. The models evaluated to estimate the moisture content might be affected by errors in the estimation in some moisture content intervals due to limits in the range of data used to train the model (Shah et al., 2019). Indeed, small increases in RF models performance were found when the models were trained with the specific season and location datasets. This difference is due to different models' accuracy when the moisture content is <30%. During the two seasons, many hybrids did not reach such low moisture content, and thus, the training set size for this interval was lower.

To assess the performance of the models in identifying the optimal harvest dates based on moisture content at different endpoints of drying, the moisture content dataset was indeed divided into different intervals (<30%, 30–60, >60%, and 10–80%). It is considered that the optimal moisture content for the *Miscanthus* winter harvest is at or below 20% (Lewandowski et al., 2016) in order to avoid self-ignition of biomass, minimize transport costs, and increase combustion efficiency (Robson et al., 2011). In this study, especially novel interspecies seed-based *M. sin x M. sac* hybrids rarely reached at harvest a moisture content lower than 30% (Figure 2), while *M. sin x M. sin* in some cases dried until 10%. In the low moisture content interval (<30%), a large difference in RMSE was found between the model trained with the reference dataset and on the season–location-specific datasets (Table 3). These results indicate that the tested models cannot be transferred with good accuracy to locations and or/growing seasons where biomass of these genotypes dried until moisture content <30%. The low transferability of RF beyond the extreme values of the training data range confirmed that this is one of the main limits of the RF model (Johansen et al., 2020; Vuolo et al., 2013). On the contrary, the RF models were transferable in different locations and growing seasons for moisture content values ranging between 30% and 60% (Table 3). The training set size and the moisture content distribution during senescence confirmed to be the most important dataset's characteristics to achieve good model's performances (Millard & Richardson, 2015) and transferability (Johansen et al., 2020).

The addition of categorical variables in RF model improved the estimation of moisture content. Introducing three categorical variables such as material, hybrid, and genotype decreased more the RMSE than adding only material type (Figure 4b,e). The *M. sin x M. sac* and *M. x giganteus* genotypes showed the highest improvement of RMSE due to the addition of these categorical variables (Figure 4f). The data imbalance in the "hybrid"

categorical variables among control *M. x giganteus* ($n = 1$), interspecies ($n = 4$), and intraspecies ($n = 8$) genotype hybrids could have caused these differences in model's performance.

Another limitation of the RF model developed in this study relies on the fact that it is composed of multiple VIs calculated with precise multispectral bands. This means that our RF model might not reach the same accuracy if the same VIs are calculated on spectral data acquired with different multispectral cameras operating within different band intervals. This calls for the development of algorithms able to overcome these differences in the spectral data through advanced normalization and calculation procedures of VIs from different sensors (Emilien et al., 2021; Hoque & Phinn, 2018).

4.3 | Phenotyping stay-green trait via UAV remote sensing to capture genotypic variation during senescence

This study demonstrated that high-throughput plant phenotyping (HTPP) of contrasting *Miscanthus* hybrids is possible by combining multiple UAV flights and GAM modeling. Stay-green (SG) is an important phenotypic trait when evaluating the senescence of novel *Miscanthus* hybrids. The goal of plant breeders is to obtain high yielding plants with high biomass quality. In *Miscanthus*, a delayed senescence is expected to increase yields, while an early senescence is expected to increase biomass quality (Robson et al., 2011). In our environments, senescence of *M. sin x M. sin* hybrids led to drier biomass (22% mean moisture content in late February) than commercially available rhizome-based hybrids (GRC 9–15 with 37%), while *M. sin x M. sac* hybrids showed an SG trait with an average moisture content of 45% until harvest. These findings confirmed that biomass with low moisture content at the harvest is usually related to early senescence in *Miscanthus*, as was found by Robson et al. (2011). However, opposite results to our study were reported by Nunn et al. (2017) that observed a lack of relationship between an early senescence and low moisture content at harvest in different locations across Europe.

Mild cold conditions during autumn–winter periods affected the start of senescence and moisture content losses dynamics until late winter harvest in all *Miscanthus* hybrids. The overwintering conditions (e.g., number and frequency of chilling frosts) between the start of senescence and harvest time have a higher effect on the moisture content than the senescence itself (Sarath et al., 2014). That was the case in our two southern European locations, where a reduced frequency of killing frost days and absence of prolonged freezing periods in late autumn–early
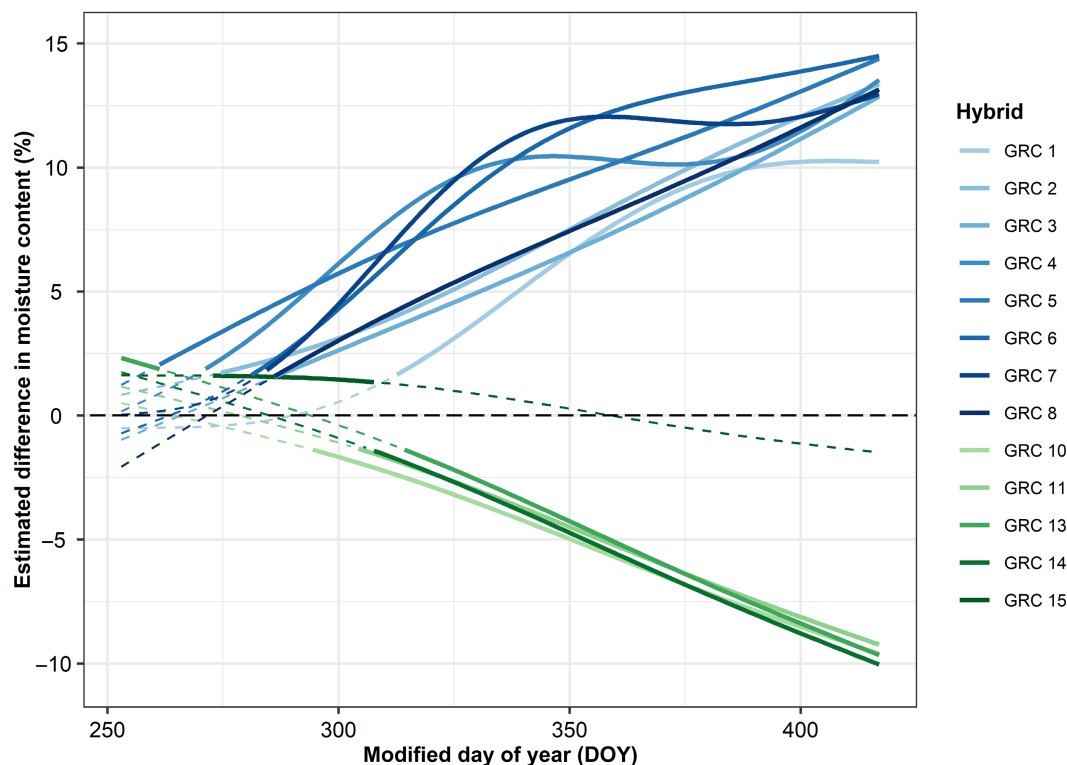
FIGURE 5 Senescence dynamics of the different *Miscanthus* hybrids according to the difference in estimated moisture content with reference hybrid *M. x giganteus*—GRC 9 (dashed black line). The estimation of moisture content time series was carried out by using a GAM. Solid and dashed coloured lines denote respectively significant ($p < 0.05$) and not significant differences of the corresponding hybrid compared to reference hybrid

winter in 2019–2020 seasons (Table 1) might not have induced complete senescence in the *M. sin x M. sac* hybrids leading to a higher moisture content at harvest. During the first years after establishment, *Miscanthus* might have a reduced senescence (Clifton-Brown & Lewandowski, 2000) due to changes in the source–sink dynamics of young *Miscanthus* plants (Boersma et al., 2015). However, standing age did not affect in our case the observed delayed senescence since measurements were done on mature plantation at second and third year.

Genotypic variations in flowering and senescence times are instead two key explanatory factors of SG trait observed in perennial crops. The relationship between flowering and senescence in *Miscanthus* has been proposed to promote nutrient remobilization, and hence biomass quality improvement (Jensen et al., 2016). GAM applied to estimated moisture content values from the RF model from multiple UAV flights helped us to capture differences in senescence dynamics in contrasting *Miscanthus* hybrids (Figure 5). A constant increase in the differences between the estimated moisture content of interspecies *M. sin x M. sac* and intraspecies *M. sin x M. sin* hybrids was observed between DOY 300 (late October) and DOY 350 (mid-December). During this period, the mean temperature decreased under 10°C. Therefore, under these mean

temperature conditions, *M. sin x M. sin* hybrids might be more sensitive to temperatures below 10°C and thus start active senescence sooner than *M. x giganteus* and *M. sin x M. sac* hybrids that instead showed a delayed senescence. Fonteyne et al. (2016) reviewed the effect of frost and chilling stress in *Miscanthus* genotypes and found that *M. sacchariflorus* was more resistant to cold stress than *M. sinensis*. All *M. sin x M. sac* genotype hybrids showed a more persistent SG compared to *M. x giganteus* and *M. sin x M. sin* hybrids. In agreement with our results, Rusinowski et al. (2019) found that *GNT 34* hybrid (GRC 13 in this study) had a longer SG period than *M. x giganteus*. Only GRC 15 among *M. sin x M. sac* genotype had similar senescence dynamics to the *M. x giganteus*. The similar senescence dynamics observed for these two commercially available rhizome-based hybrids confirm that transplanting material (rhizome vs. seed-based plugs) has an impact on moisture content loss during senescence. The observed differences in senescence time and moisture content loss rate during senescence among *Miscanthus* genotypes are, respectively, linked to flowering time and nutrient remobilization. Other studies confirming that *M. sin x M. sin* hybrids flowered earlier (mid-summer) than rhizome-based *M. x giganteus* hybrid while *M. sin x M. sac* never reached flowering (Clifton-Brown & Lewandowski, 2002;

Nunn et al., 2017). Jensen et al. (2016) found, for similar contrasting hybrids, that nitrogen and phosphorous re-mobilization rate to underground rhizomes followed the same trend of moisture content loss observed also in our study. The absence or delay of flowering, respectively, in *M. sin x M. sac* and rhizome-based hybrids may have caused delayed senescence that was also observed in the SG trait in this study. As a consequence, these genotypes were harvested at higher moisture content (Figure S1) and likely higher nutrient content compared to *M. sin x M. sin* hybrids. The high variability among *Miscanthus* hybrids in moisture content loss dynamics during senescence (Figure 5) might be further explained by the wider geographical distribution of *M. sinensis* than of *M. sacchariflorus* (Clifton-Brown & Hastings, 2015). This may have produced a higher genetic variation of the phenotypic traits due to the hybridization among *M. sinensis* species (Robson et al., 2011). Additionally, also the cold resistance trait likely depends on the origin and in situ environmental characteristics of the genetic accession of the *Miscanthus* species. In fact, opposite results to our study were reported by Clifton-Brown et al. (2002) showing that different *M. sin x M. sin* hybrids had delayed senescence with respect to *M. x giganteus* and *M. sacchariflorus* hybrids.

In conclusion, this study demonstrated that moisture content of *Miscanthus* can be accurately estimated via machine learning algorithm applied to multiple VIs calculated from UAV-based VIS-NIR images. The RF model developed on different genotypes showed a good transferability to multiple location and seasons when moisture content ranges from 30% to 60%. Further training datasets are required to extend the transferability and confirm the same performance of the RF model at lower moisture content values (10%–30%). For the first time, we showed that the combination of machine learning (ML) and GAM applied to time series of moisture content values estimated from VIs derived from multiple UAV flights is a powerful tool for high-throughput plant phenotyping. Remote sensing can be used for phenotyping future advanced breeding programs of *Miscanthus*. The possibility to distinguish via remote sensing the SG trait of novel *Miscanthus* hybrids can deepen our understanding of key factors mediating the induction of early or delayed senescence. Our study focused on the use of ML algorithms to estimate moisture content during *Miscanthus* senescence, but we believe that the same methodological approach can be used for estimating other phenological traits or yield components in similar and/or different crops. This is particularly relevant for upscaling models from experimental plot to field scale by using satellites. Satellites can collect data of many fields simultaneously, with a larger number of spectral bands, like the SWIR band, that could ultimately support with high precision and resolution moisture content and yield estimation. ML algorithms could be applied in remote sensing to develop satellite and UAV applications beneficial to sustainable crop management, for example, in the case of *Miscanthus* to identify optimal harvest date or to predict commercial yield (quantity and quality).

CONFLICTS OF INTEREST
Authors declare no conflicts of interest.

AUTHORS CONTRIBUTION
S.A. led the project; G.I., M.C., A.F., and S.A. involved in the conceptualization of the study; G.I. and M.C. involved in methodology and UAV spectral image acquisitions; G.I. involved in writing—original draft preparation, data analysis, and images analysis; G.I., M.C., and E.M. involved in field measurements; A.F., E.M., and S.A. involved in review and editing; J.K. provided GRC 15 hybrid; L.T. provided the *M. sinensis x M. sinensis* hybrids; and J.C.B. provided the *M. sinensis x M. sacchariflorus* hybrids used to set up the field trial. All authors have read and agreed to the published version of the manuscript.

DATA AVAILABILITY STATEMENT
The data that support the findings of this work are openly available in the Zenodo data repository (https://zenodo.org/) at https://doi.org/10.5281/zenodo.6053788.

ORCID
Giorgio Impollonia https://orcid.org/0000-0002-9878-6595
Michele Croci https://orcid.org/0000-0001-7356-2774
Enrico Martani https://orcid.org/0000-0003-0236-0328
Andrea Ferrarini https://orcid.org/0000-0001-9390-7004
Luisa M. Trindade https://orcid.org/0000-0003-1541-2094
John Clifton-Brown https://orcid.org/0000-0001-6477-5452
Stefano Amaducci https://orcid.org/0000-0002-6184-9257

REFERENCES
Agostini, A., Serra, P., Giuntoli, J., Martani, E., Ferrarini, A., & Amaducci, S. (2021). Biofuels from perennial energy crops on buffer strips: A win-win strategy. *Journal of Cleaner Production*, *297*, 126703. https://doi.org/10.1016/j.jclepro.2021.126703

Alam, M. M., Strandgard, M. N., Brown, M. W., & Fox, J. C. (2012). Improving the productivity of mechanised harvesting systems using remote sensing. *Australian Forestry*, *75*(4), 238–245. https://doi.org/10.1080/00049158.2012.10676408

Alexandridis, T. K., Ovakoglou, G., & Clevers, J. G. P. W. (2019). Relationship between MODIS EVI and LAI across time and space. *Geocarto International*, *35*(13), 1385–1399. https://doi.org/10.1080/10106049.2019.1573928

Amaducci, S., Facciotto, G., Bergante, S., Perego, A., Serra, P., Ferrarini, A., & Chimento, C. (2016). Biomass production and energy balance of herbaceous and woody crops on marginal soils in the Po Valley. *GCB Bioenergy*, *9*(1), 31–45. https://doi.org/10.1111/gcbb.12341

Anderegg, J., Yu, K., Aasen, H., Walter, A., Liebisch, F., & Hund, A. (2020). Spectral vegetation indices to track senescence dynamics in diverse wheat germplasm. *Frontiers in Plant Science*, *10*. https://doi.org/10.3389/fpls.2019.01749

Antonucci, G., Croci, M., Miras-Moreno, B., Fracasso, A., & Amaducci, S. (2021). Integration of gas exchange with metabolomics: High-throughput phenotyping methods for screening biostimulant-elicited beneficial responses to short-term water deficit. *Frontiers in Plant Science*, *12*. https://doi.org/10.3389/fpls.2021.678925

Belgiu, M., & Drăguţ, L. (2016). Random forest in remote sensing: A review of applications and future directions. *ISPRS Journal of Photogrammetry and Remote Sensing*, *114*, 24–31. https://doi.org/10.1016/j.isprsjprs.2016.01.011

Blancon, J., Dutartre, D., Tixier, M.-H., Weiss, M., Comar, A., Praud, S., & Baret, F. (2019). A high-throughput model-assisted method for phenotyping maize green leaf area index dynamics using unmanned aerial vehicle imagery. *Frontiers in Plant Science*, *10*. https://doi.org/10.3389/fpls.2019.00685

Boersma, N. N., Dohleman, F. G., Miguez, F. E., & Heaton, E. A. (2015). Autumnal leaf senescence in Miscanthus × giganteus and leaf [N] differ by stand age. *Journal of Experimental Botany*, *66*(14), 4395–4401. https://doi.org/10.1093/jxb/erv129

Bogard, M., Jourdan, M., Allard, V., Martre, P., Perretant, M. R., Ravel, C., Heumez, E., Orford, S., Snape, J., Griffiths, S., Gaju, O., Foulkes, J., & Le Gouis, J. (2011). Anthesis date mainly explained correlations between post-anthesis leaf senescence, grain yield, and grain protein concentration in a winter wheat population segregating for flowering time QTLs. *Journal of Experimental Botany*, *62*(10), 3621–3636. https://doi.org/10.1093/jxb/err061

Cabrera-Bosquet, L., Molero, G., Stellacci, A., Bort, J., Nogués, S., & Araus, J. (2011). NDVI as a potential tool for predicting biomass, plant nitrogen content and growth in wheat genotypes subjected to different water and nitrogen conditions. *Cereal Research Communications*, *39*(1), 147–159. https://doi.org/10.1556/crc.39.2011.1.15

Cerrudo, D., González Pérez, L., Mendoza Lugo, J., & Trachsel, S. (2017). Stay-green and associated vegetative indices to breed maize adapted to heat and combined heat-drought stresses. *Remote Sensing*, *9*(3), 235. https://doi.org/10.3390/rs9030235

Christopher, J. T., Veyradier, M., Borrell, A. K., Harvey, G., Fletcher, S., & Chenu, K. (2014). Phenotyping novel stay-green traits to capture genetic variation in senescence dynamics. *Functional Plant Biology*, *41*(11), 1035. https://doi.org/10.1071/fp14052

Clifton-Brown, J., Harfouche, A., Casler, M. D., Dylan Jones, H., Macalpine, W. J., Murphy-Bokern, D., Smart, L. B., Adler, A., Ashman, C., Awty-Carroll, D., Bastien, C., Bopper, S., Botnari, V., Brancourt-Hulmel, M., Chen, Z., Clark, L. V., Cosentino, S., Dalton, S., Davey, C., … Lewandowski, I. (2018). Breeding progress and preparedness for mass-scale deployment of perennial lignocellulosic biomass crops switchgrass, miscanthus, willow and poplar. *GCB Bioenergy*, *11*(1), 118–151. https://doi.org/10.1111/gcbb.12566

Clifton-Brown, J. C., & Lewandowski, I. (2000). Overwintering problems of newly established Miscanthus plantations can be overcome by identifying genotypes with improved rhizome cold tolerance. *New Phytologist*, *148*(2), 287–294. https://doi.org/10.1046/j.1469-8137.2000.00764.x

Clifton-Brown, J. C., & Lewandowski, I. (2002). Screening Miscanthus genotypes in field trials to optimise biomass yield and quality in Southern Germany. *European Journal of Agronomy*, *16*(2), 97–110. https://doi.org/10.1016/s1161-0301(01)00120-4

Clifton-Brown, J. C., Lewandowski, I., Andersson, B., Basch, G., Christian, D. G., Kjeldsen, J. B., J⊘rgensen, U., Mortensen, J. V., Riche, A. B., Schwarz, K.-U., Tayebi, K., & Teixeira, F. (2001). Performance of 15 Miscanthus genotypes at five sites in Europe. *Agronomy Journal*, *93*(5), 1013–1019. https://doi.org/10.2134/agronj2001.9351013x

Clifton-Brown, J. C., Lewandowski, I., Bangerth, F., & Jones, M. B. (2002). Comparative responses to water stress in stay-green, rapid- and slow senescing genotypes of the biomass crop, Miscanthus. *New Phytologist*, *154*(2), 335–345. https://doi.org/10.1046/j.1469-8137.2002.00381.x

Clifton-Brown, J., Schwarz, K.-U., Awty-Carroll, D., Iurato, A., Meyer, H., Greef, J., Gwyn, J., Mos, M., Ashman, C., Hayes, C., Huang, L., Norris, J., Rodgers, C., Scordia, D., Shafiei, R., Squance, M., Swaller, T., Youell, S., Cosentino, S., … Robson, P. (2019). Breeding strategies to improve Miscanthus as a sustainable source of biomass for bioenergy and biorenewable products. *Agronomy*, *9*(11), 673. https://doi.org/10.3390/agronomy9110673

Clifton-Brown, S., & Hastings, A. (2015). History of the development of Miscanthus as a bioenergy crop: From small beginnings to potential realisation. *Biology and Environment: Proceedings of the Royal Irish Academy*, *115B*(1), 45. https://doi.org/10.3318/bioe.2015.05

Emilien, A.-V., Thomas, C., & Thomas, H. (2021). UAV & satellite synergies for optical remote sensing applications: A literature review. In *Science of remote sensing* (vol. 3, p. 100019). Elsevier BV. https://doi.org/10.1016/j.srs.2021.100019

Feng, L., Zhang, Z., Ma, Y., Du, Q., Williams, P., Drewry, J., & Luck, B. (2020). Alfalfa yield prediction using UAV-based hyperspectral imagery and ensemble learning. *Remote Sensing*, *12*(12), 2028. https://doi.org/10.3390/rs12122028

Ferrarini, A., Fornasier, F., Serra, P., Ferrari, F., Trevisan, M., & Amaducci, S. (2016). Impacts of willow and miscanthus bioenergy buffers on biogeochemical N removal processes along the soil-groundwater continuum. *GCB Bioenergy*, *9*(1), 246–261. https://doi.org/10.1111/gcbb.12340

Ferrarini, A., Martani, E., Fornasier, F., & Amaducci, S. (2021). High C input by perennial energy crops boosts belowground functioning and increases soil organic P content. *Agriculture, Ecosystems & Environment*, *308*, 107247. https://doi.org/10.1016/j.agee.2020.107247

Fonteyne, S., Roldán-Ruiz, I., Muylle, H., De Swaef, T., Reheul, D., & Lootens, P. (2016). A review of frost and chilling stress in

Miscanthus and its importance to biomass yield. In *Perennial biomass crops for a resource-constrained world* (pp. 127–144). Springer International Publishing. https://doi.org/10.1007/978-3-319-44530-4_12

Furbank, R. T., & Tester, M. (2011). Phenomics – Technologies to relieve the phenotyping bottleneck. *Trends in Plant Science*, *16*(12), 635–644. https://doi.org/10.1016/j.tplants.2011.09.005

Gao, B. (1996). NDWI—A normalized difference water index for remote sensing of vegetation liquid water from space. *Remote Sensing of Environment*, *58*(3), 257–266. https://doi.org/10.1016/s0034-4257(96)00067-3

Gracia-Romero, A., Kefauver, S. C., Fernandez-Gallego, J. A., Vergara-Díaz, O., Nieto-Taladriz, M. T., & Araus, J. L. (2019). UAV and ground image-based phenotyping: A proof of concept with durum wheat. *Remote Sensing*, *11*(10), 1244. https://doi.org/10.3390/rs11101244

Haboudane, D., Miller, J. R., Tremblay, N., Zarco-Tejada, P. J., & Dextraze, L. (2002). Integrated narrow-band vegetation indices for prediction of crop chlorophyll content for application to precision agriculture. *Remote Sensing of Environment*, *81*(2–3), 416–426. https://doi.org/10.1016/s0034-4257(02)00018-4

Han, L., Yang, G., Dai, H., Xu, B., Yang, H., Feng, H., Li, Z., & Yang, X. (2019). Modeling maize above-ground biomass based on machine learning approaches using UAV remote-sensing data. *Plant Methods*, *15*(1). https://doi.org/10.1186/s13007-019-0394-z

Hassan, M., Yang, M., Rasheed, A., Jin, X., Xia, X., Xiao, Y., & He, Z. (2018). Time-series multispectral indices from unmanned aerial vehicle imagery reveal senescence rate in bread wheat. *Remote Sensing*, *10*(6), 809. https://doi.org/10.3390/rs10060809

Hastings, A., Mos, M., Yesufu, J. A., McCalmont, J., Schwarz, K., Shafei, R., Ashman, C., Nunn, C., Schuele, H., Cosentino, S., Scalici, G., Scordia, D., Wagner, M., & Clifton-Brown, J. (2017). Economic and environmental assessment of seed and rhizome propagated Miscanthus in the UK. *Frontiers in Plant Science*, *8*, 1058. https://doi.org/10.3389/FPLS.2017.01058

Heaton, E. A., Dohleman, F. G., Miguez, A. F., Juvik, J. A., Lozovaya, V., Widholm, J., Zabotina, O. A., McIsaac, G. F., David, M. B., Voigt, T. B., Boersma, N. N., & Long, S. P. (2010). Miscanthus. In *Advances in botanical research* (pp. 75–137). Elsevier. https://doi.org/10.1016/b978-0-12-381518-7.00003-0

Hodkinson, T. R., Chase, M. W., & Renvoize, S. A. (2002). Characterization of a genetic resource collection for Miscanthus (Saccharinae, Andropogoneae, Poaceae) using AFLP and ISSR PCR. *Annals of Botany*, *89*(5), 627–636. https://doi.org/10.1093/AOB/MCF091

Holloway, J., & Mengersen, K. (2018). Statistical machine learning methods and remote sensing for sustainable development goals: A review. *Remote Sensing*, *10*(9), 1365. https://doi.org/10.3390/rs10091365

Hoque, M.-A.-A., & Phinn, S. (2018). Methods for linking drone and field hyperspectral data to satellite data. In *Fundamentals, sensor systems, spectral libraries, and data mining for vegetation* (pp. 321–354). CRC Press. https://doi.org/10.1201/9781315164151-12

Im, J., Jensen, J. R., Coleman, M., & Nelson, E. (2009). Hyperspectral remote sensing analysis of short rotation woody crops grown with controlled nutrient and irrigation treatments. *Geocarto International*, *24*(4), 293–312. https://doi.org/10.1080/10106040802556207

Jackson, T. J., Chen, D., Cosh, M., Li, F., Anderson, M., Walthall, C., Doriaswamy, P., & Hunt, E. R. (2004). Vegetation water content mapping using Landsat data derived normalized difference water index for corn and soybeans. *Remote Sensing of Environment*, *92*(4), 475–482. https://doi.org/10.1016/J.RSE.2003.10.021

Jensen, E., Robson, P., Farrar, K., Thomas Jones, S., Clifton-Brown, J., Payne, R., & Donnison, I. (2016). Towards Miscanthus combustion quality improvement: The role of flowering and senescence. *GCB Bioenergy*, *9*(5), 891–908. https://doi.org/10.1111/gcbb.12391

Johansen, K., Morton, M. J. L., Malbeteau, Y., Aragon, B., Al-Mashharawi, S., Ziliani, M. G., Angel, Y., Fiene, G., Negrão, S., Mousa, M. A. A., Tester, M. A., & McCabe, M. F. (2020). Predicting biomass and yield in a tomato phenotyping experiment using UAV imagery and random forest. *Frontiers in Artificial Intelligence*, *3*. https://doi.org/10.3389/frai.2020.00028

Kamir, E., Waldner, F., & Hochman, Z. (2020). Estimating wheat yields in Australia using climate records, satellite image time series and machine learning methods. *ISPRS Journal of Photogrammetry and Remote Sensing*, *160*, 124–135. https://doi.org/10.1016/j.isprsjprs.2019.11.008

Kavats, O., Khramov, D., Sergieieva, K., & Vasyliev, V. (2019). Monitoring harvesting by time series of Sentinel-1 SAR data. *Remote Sensing*, *11*(21), 2496. https://doi.org/10.3390/rs11212496

Kipp, S., Mistele, B., & Schmidhalter, U. (2014). Identification of stay-green and early senescence phenotypes in high-yielding winter wheat, and their relationship to grain yield and grain protein concentration using high-throughput phenotyping techniques. *Functional Plant Biology*, *41*(3), 227. https://doi.org/10.1071/fp13221

Kuhn, M. (2008). Building predictive models in R using the caret Package. *Journal of Statistical Software*, *28*(5). https://doi.org/10.18637/jss.v028.i05

Kuhn, M., & Johnson, K. (2013). *Applied predictive modeling*. Springer. https://doi.org/10.1007/978-1-4614-6849-3

Lewandowski, I., Clifton-Brown, J., Trindade, L. M., van der Linden, G. C., Schwarz, K.-U., Müller-Sämann, K., Anisimov, A., Chen, C.-L., Dolstra, O., Donnison, I. S., Farrar, K., Fonteyne, S., Harding, G., Hastings, A., Huxley, L. M., Iqbal, Y., Khokhlov, N., Kiesel, A., Lootens, P., ... Kalinina, O. (2016). Progress on optimizing Miscanthus biomass production for the European bioeconomy: Results of the EU FP7 project OPTIMISC. *Frontiers in Plant Science*, *7*. https://doi.org/10.3389/fpls.2016.01620

Li, H., Yang, W., Lei, J., She, J., & Zhou, X. (2021). Estimation of leaf water content from hyperspectral data of different plant species by using three new spectral absorption indices. *PLoS One*, *16*(3), e0249351. https://doi.org/10.1371/journal.pone.0249351

Liedtke, J. D., Hunt, C. H., George-Jaeggli, B., Laws, K., Watson, J., Potgieter, A. B., Cruickshank, A., & Jordan, D. R. (2020). High-throughput phenotyping of dynamic canopy traits associated with stay-green in grain sorghum. *Plant Phenomics*, *2020*, 1–10. https://doi.org/10.34133/2020/4635153

Lopes, M. S., & Reynolds, M. P. (2012). Stay-green in spring wheat can be determined by spectral reflectance measurements (normalized difference vegetation index) independently from phenology. *Journal of Experimental Botany*, *63*(10), 3789–3798. https://doi.org/10.1093/jxb/ers071

Makanza, R., Zaman-Allah, M., Cairns, J., Magorokosho, C., Tarekegne, A., Olsen, M., & Prasanna, B. (2018).

High-throughput phenotyping of canopy cover and senescence in maize field trials using aerial digital canopy imaging. *Remote Sensing*, *10*(2), 330. https://doi.org/10.3390/rs10020330

Malinowska, M., Donnison, I. S., & Robson, P. R. H. (2016). Phenomics analysis of drought responses in Miscanthus collected from different geographical locations. *GCB Bioenergy*, *9*(1), 78–91. https://doi.org/10.1111/gcbb.12350

Martani, E., Ferrarini, A., Serra, P., Pilla, M., Marcone, A., & Amaducci, S. (2021). Belowground biomass C outweighs soil organic C of perennial energy crops: Insights from a long-term multispecies trial. *GCB Bioenergy*, *13*(3), 459–472. https://doi.org/10.1111/gcbb.12785

Maxwell, A. E., Warner, T. A., & Fang, F. (2018). Implementation of machine-learning classification in remote sensing: An applied review. *International Journal of Remote Sensing*, *39*(9), 2784–2817. https://doi.org/10.1080/01431161.2018.1433343

Meroni, M., Waldner, F., Seguini, L., Kerdiles, H., & Rembold, F. (2021). Yield forecasting with machine learning and small data: What gains for grains? *Agricultural and Forest Meteorology*, *308–309*, 108555. https://doi.org/10.1016/j.agrformet.2021.108555

Merzlyak, M. N., Gitelson, A. A., Chivkunova, O. B., & Rakitin, V. Y. U. (1999). Non-destructive optical detection of pigment changes during leaf senescence and fruit ripening. *Physiologia Plantarum*, *106*(1), 135–141. https://doi.org/10.1034/j.1399-3054.1999.106119.x

Millard, K., & Richardson, M. (2015). On the importance of training data sample selection in random forest image classification: A case study in peatland ecosystem mapping. *Remote Sensing*, *7*(7), 8489–8515. https://doi.org/10.3390/rs70708489

Munaiz, E. D., Martínez, S., Kumar, A., Caicedo, M., & Ordás, B. (2020). The senescence (stay-green)—An important trait to exploit crop residuals for bioenergy. *Energies*, *13*(4), 790. https://doi.org/10.3390/en13040790

Nolè, A., Rita, A., Ferrara, A. M. S., & Borghetti, M. (2018). Effects of a large-scale late spring frost on a beech (*Fagus sylvatica* L.) dominated Mediterranean mountain forest derived from the spatio-temporal variations of NDVI. *Annals of Forest Science*, *75*(3). https://doi.org/10.1007/s13595-018-0763-1

Nunn, C., Hastings, A. F., St, J., Kalinina, O., Özgüven, M., Schüle, H., Tarakanov, I. G., Van Der Weijde, T., Anisimov, A. A., Iqbal, Y., Kiesel, A., Khokhlov, N. F., McCalmont, J. P., Meyer, H., Mos, M., Schwarz, K.-U., Trindade, L. M., Lewandowski, I., & Clifton-Brown, J. C. (2017). Environmental influences on the growing season duration and ripening of diverse Miscanthus germplasm grown in six countries. *Frontiers in Plant Science*, *8*. https://doi.org/10.3389/fpls.2017.00907

Ostos-Garrido, F. J., de Castro, A. I., Torres-Sánchez, J., Pistón, F., & Peña, J. M. (2019). High-throughput phenotyping of bioethanol potential in cereals using UAV-based multi-spectral imagery. *Frontiers in Plant Science*, *10*. https://doi.org/10.3389/fpls.2019.00948

Pancaldi, F., & Trindade, L. M. (2020). Marginal lands to grow novel bio-based crops: A plant breeding perspective. *Frontiers in Plant Science*, *11*. https://doi.org/10.3389/fpls.2020.00227

Parmley, K. A., Higgins, R. H., Ganapathysubramanian, B., Sarkar, S., & Singh, A. K. (2019). Machine learning approach for prescriptive plant breeding. *Scientific Reports*, *9*(1). https://doi.org/10.1038/s41598-019-53451-4

Peñuelas, J., Baret, F., & Filella, I. (1995). Semiempirical indexes to assess carotenoids chlorophyll-a ratio from leaf spectral reflectance. *Photosynthetica*, *31*, 221–230.

Peñuelas, J., & Inoue, Y. (1999). Reflectance indices indicative of changes in water and pigment contents of peanut and wheat leaves. *Photosynthetica*, *36*(3), 355–360. https://doi.org/10.1023/a:1007033503276

Potgieter, A. B., George-Jaeggli, B., Chapman, S. C., Laws, K., Suárez Cadavid, L. A., Wixted, J., Watson, J., Eldridge, M., Jordan, D. R., & Hammer, G. L. (2017). Multi-spectral imaging from an unmanned aerial vehicle enables the assessment of seasonal leaf area dynamics of sorghum breeding lines. *Frontiers in Plant Science*, *8*. https://doi.org/10.3389/fpls.2017.01532

QGIS Development Team. (2021). QGIS (Version 3.18-Zurich). Open Source Geospatial Foundation Project. https://qgis.org/en/site/

Robson, P., Mos, M., Clifton-Brown, J., & Donnison, I. (2011). Phenotypic variation in senescence in Miscanthus: Towards optimising biomass quality and quantity. *BioEnergy Research*, *5*(1), 95–105. https://doi.org/10.1007/s12155-011-9118-6

Rusinowski, S., Krzyżak, J., Clifton-Brown, J., Jensen, E., Mos, M., Webster, R., Sitko, K., & Pogrzeba, M. (2019). New Miscanthus hybrids cultivated at a Polish metal-contaminated site demonstrate high stomatal regulation and reduced shoot Pb and Cd concentrations. *Environmental Pollution*, *252*, 1377–1387. https://doi.org/10.1016/j.envpol.2019.06.062

Samuelsson, R., Burvall, J., & Jirjis, R. (2006). Comparison of different methods for the determination of moisture content in biomass. *Biomass and Bioenergy*, *30*(11), 929–934. https://doi.org/10.1016/j.biombioe.2006.06.004

Sarath, G., Baird, L. M., & Mitchell, R. B. (2014). Senescence, dormancy and tillering in perennial C4 grasses. *Plant Science*, *217–218*, 140–151. https://doi.org/10.1016/j.plantsci.2013.12.012

Schauberger, B., Jägermeyr, J., & Gornott, C. (2020). A systematic review of local to regional yield forecasting approaches and frequently used data resources. *European Journal of Agronomy*, *120*, 126153. https://doi.org/10.1016/j.eja.2020.126153

Shah, S. H., Angel, Y., Houborg, R., Ali, S., & McCabe, M. F. (2019). A random forest machine learning approach for the retrieval of leaf chlorophyll content in wheat. *Remote Sensing*, *11*(8), 920. https://doi.org/10.3390/rs11080920

Shepherd, A., Clifton-Brown, J., Kam, J., Buckby, S., & Hastings, A. (2020). Commercial experience with miscanthus crops: Establishment, yields and environmental observations. *GCB Bioenergy*, *12*(7), 510–523. https://doi.org/10.1111/gcbb.12690

Styks, J., Wróbel, M., Frączek, J., & Knapczyk, A. (2020). Effect of compaction pressure and moisture content on quality parameters of perennial biomass pellets. *Energies*, *13*(8), 1859. https://doi.org/10.3390/en13081859

Su, W., Zhang, M., Bian, D., Liu, Z., Huang, J., Wang, W., Wu, J., & Guo, H. (2019). Phenotyping of corn plants using unmanned aerial vehicle (UAV) images. *Remote Sensing*, *11*(17), 2021. https://doi.org/10.3390/rs11172021

Thomas, H., & Howarth, C. J. (2000). Five ways to stay green. *Journal of Experimental Botany*, *51*(suppl_1), 329–337. https://doi.org/10.1093/jexbot/51.suppl_1.329

van der Cruijsen, K., Al Hassan, M., van Erven, G., Dolstra, O., & Trindade, L. M. (2021). Breeding targets to improve biomass quality in Miscanthus. *Molecules*, *26*(2), 254. https://doi.org/10.3390/molecules26020254

Varela, S., Pederson, T., Bernacchi, C. J., & Leakey, A. D. B. (2021). Understanding growth dynamics and yield prediction of sorghum using high temporal resolution UAV imagery time series

and machine learning. *Remote Sensing*, *13*(9), 1763. https://doi.org/10.3390/rs13091763

Verrelst, J., Camps-Valls, G., Muñoz-Marí, J., Rivera, J. P., Veroustraete, F., Clevers, J. G. P. W., & Moreno, J. (2015). Optical remote sensing and the retrieval of terrestrial vegetation bio-geophysical properties – A review. *ISPRS Journal of Photogrammetry and Remote Sensing*, *108*, 273–290. https://doi.org/10.1016/j.isprsjprs.2015.05.005

Verrelst, J., Malenovský, Z., Van der Tol, C., Camps-Valls, G., Gastellu-Etchegorry, J.-P., Lewis, P., North, P., & Moreno, J. (2018). Quantifying vegetation biophysical variables from imaging spectroscopy data: A Review on retrieval methods. *Surveys in Geophysics*, *40*(3), 589–629. https://doi.org/10.1007/s10712-018-9478-y

Vuolo, F., Neugebauer, N., Bolognesi, S., Atzberger, C., & D'Urso, G. (2013). Estimation of leaf area index using DEIMOS-1 data: Application and transferability of a semi-empirical relationship between two agricultural areas. *Remote Sensing*, *5*(3), 1274–1291. https://doi.org/10.3390/rs5031274

Wang, J., Badenhorst, P., Phelan, A., Pembleton, L., Shi, F., Cogan, N., Spangenberg, G., & Smith, K. (2019). Using sensors and unmanned aircraft systems for high-throughput phenotyping of biomass in perennial ryegrass breeding trials. *Frontiers in Plant Science*, *10*. https://doi.org/10.3389/fpls.2019.01381

Wolanin, A., Mateo-García, G., Camps-Valls, G., Gómez-Chova, L., Meroni, M., Duveiller, G., Liangzhi, Y., & Guanter, L. (2020). Estimating and understanding crop yields with explainable deep learning in the Indian Wheat Belt. *Environmental Research Letters*, *15*(2), 024019. https://doi.org/10.1088/1748-9326/ab68ac

Wood, S. N. (2017). *Generalized additive models*. Chapman and Hall/CRC. https://doi.org/10.1201/9781315370279

Xie, C., & Yang, C. (2020). A review on plant high-throughput phenotyping traits using UAV-based sensors. *Computers and Electronics in Agriculture*, *178*, 105731. https://doi.org/10.1016/j.compag.2020.105731

Xie, Q., Mayes, S., & Sparkes, D. L. (2016). Early anthesis and delayed but fast leaf senescence contribute to individual grain dry matter and water accumulation in wheat. *Field Crops Research*, *187*, 24–34. https://doi.org/10.1016/j.fcr.2015.12.009

Yang, G., Liu, J., Zhao, C., Li, Z., Huang, Y., Yu, H., Xu, B., Yang, X., Zhu, D., Zhang, X., Zhang, R., Feng, H., Zhao, X., Li, Z., Li, H., & Yang, H. (2017). Unmanned aerial vehicle remote sensing for field-based crop phenotyping: Current status and perspectives. *Frontiers in Plant Science*, *8*. https://doi.org/10.3389/fpls.2017.01111

Yang, H. (2011). Remote sensing technique for predicting harvest time of tomatoes. *Procedia Environmental Sciences*, *10*, 666–671. https://doi.org/10.1016/j.proenv.2011.09.107

Yang, J., & Udvardi, M. (2017). Senescence and nitrogen use efficiency in perennial grasses for forage and biofuel production. *Journal of Experimental Botany*, *69*(4), 855–865. https://doi.org/10.1093/jxb/erx241

Yu, N., Li, L., Schmitz, N., Tian, L. F., Greenberg, J. A., & Diers, B. W. (2016). Development of methods to improve soybean yield estimation and predict plant maturity with an unmanned aerial vehicle based platform. *Remote Sensing of Environment*, *187*, 91–101. https://doi.org/10.1016/j.rse.2016.10.005

Yue, J., Feng, H., Yang, G., & Li, Z. (2018). A comparison of regression techniques for estimation of above-ground winter wheat biomass using near-surface spectroscopy. *Remote Sensing*, *10*(2), 66. https://doi.org/10.3390/rs10010066

Zhang, F., & Zhou, G. (2019). Estimation of vegetation water content using hyperspectral vegetation indices: A comparison of crop water indicators in response to water stress treatments for summer maize. *BMC Ecology*, *19*(1). https://doi.org/10.1186/s12898-019-0233-0

Zhang, M., Abrahao, G., Cohn, A., Campolo, J., & Thompson, S. (2021). A MODIS-based scalable remote sensing method to estimate sowing and harvest dates of soybean crops in Mato Grosso, Brazil. *Heliyon*, *7*(7), e07436. https://doi.org/10.1016/j.heliyon.2021.e07436

Zhou, J., Yungbluth, D., Vong, C. N., Scaboo, A., & Zhou, J. (2019). Estimation of the maturity date of soybean breeding lines using UAV-based multispectral imagery. *Remote Sensing*, *11*(18), 2075. https://doi.org/10.3390/rs11182075

Zhu, W., Sun, Z., Huang, Y., Lai, J., Li, J., Zhang, J., Yang, B., Li, B., Li, S., Zhu, K., Li, Y., & Liao, X. (2019). Improving field-scale wheat LAI retrieval based on UAV remote-sensing observations and optimized VI-LUTs. *Remote Sensing*, *11*(20), 2456. https://doi.org/10.3390/rs11202456

SUPPORTING INFORMATION

Additional supporting information may be found in the online version of the article at the publisher's website.